Research Article | Vol. 29, No. 3 / 1 February 2021 / Optics Express 4530
Optics EXPRESS

Scatter-plate microscopy with spatially coherent illumination and temporal scatter modulation

STEPHAN LUDWIG,[1,*] PAVEL RUCHKA,[1] GIANCARLO PEDRINI,[1] XIANG PENG,[2] AND WOLFGANG OSTEN[1]

[1] University Stuttgart, Institut für Technische Optik, Stuttgart, 70569, Germany
[2] College of Physics and Optoelectronic Engineering, Key Laboratory of Optoelectronic Devices and Systems of Ministry of Education and Guangdong Province, Shenzhen University, Shenzhen, 518060, China
[*] ludwig@ito.uni-stuttgart.de

Abstract: Scatter-plate microscopy (SPM) is a lensless imaging technique for high-resolution imaging through scattering media. So far, the method was demonstrated for spatially incoherent illumination and static scattering media. In this publication, we demonstrate that these restrictions are not necessary. We realized imaging with spatially coherent and spatially incoherent illumination. We further demonstrate that SPM is still a valid imaging method for scatter-plates, which change their scattering behaviour (i.e. the phase-shift) at each position on the plate continuously but independently from other positions. Especially we realized imaging through rotating ground glass diffusers.

1. Introduction

Imaging through scattering media is of high interest in many research fields and can find various applications in imaging through fog, smoke [1] or turbid media [2,3], in astronomical, biological and medical imaging [4].

In recent times, many imaging techniques exploiting the memory effect of the scattering media to image through the visually opaque materials have been presented [5]. The optical memory effect describes the shift-invariance of speckle patterns when a light source illuminating a scattering surface is slightly tilted (e.g. in the case of plane wave illumination) or shifted (e.g.in the case of point source illumination) [6]. The mentioned techniques apply Fienup-type algorithms [7] on the random patterns generated by illuminating objects hidden behind scattering media [8,9] or they interferometrically focus the light through scattering media [10] or they use the knowledge of the scattering behaviour of the visually opaque medium gained with known objects [11] or a reference point source. The latter approach means the use of a previously recorded point spread function (PSF). In former publications, we demonstrated the capabilities of this approach called scatter-plate microscopy (SPM) to realize high-resolution 3D microscopic imaging [12–14]. Most publications concerning imaging based on the memory effect refer to an early publication of Isaac Freund who first described the capabilities of memory-effect based imaging [5]. However, the pure concept of Freund was so far not realized since whereas Freund proposed an imaging method for spatially coherent illumination the mentioned techniques use temporal coherent but spatially incoherent illumination. In this paper, we investigate the capability of scatter-plate microscopy with spatially coherent sample illumination. In SPM spatially incoherent illumination is usually generated by leading a laser beam through a rotating ground glass diffuser (see Fig. 4 in section 3.2). Such a setup has a low light efficiency is quite bulky and the rotating diffuser causes vibrations disturbing the microscopic imaging process.

Coherent sample illumination in turn can be realized by illuminating the sample directly with the laser beam. A further advantage of coherent illumination is that the patterns show a much higher contrast compared to the case of spatially incoherent illumination, which enables imaging with low power illumination. On the other hand, it turns out that with spatially coherent sample

#412047 https://doi.org/10.1364/OE.412047
Journal © 2021 Received 13 Oct 2020; revised 18 Dec 2020; accepted 19 Dec 2020; published 28 Jan 2021

Optics EXPRESS

illumination, either one must record a rather large part of the scatter field or the images obtained with many different scatter-plates have to be averaged, to reach the image quality of spatially incoherent SPM.

We further demonstrate that if we record the PSF and the random pattern generated by the sample simultaneously, SPM can even be applied when the scattering media is changing its scattering behaviour and not only with static scatter-plates. To estimate the capabilities of SPM we simulated the method with random phase masks applied as scatter-plates. Experimental results are presented.

2. Principles

Light transmitted by a sample in the object plane (field distribution $O(\hat{\mathbf{r}}, \hat{z})$, with $\hat{z}$ the distance to the scatter-plate and $\hat{\mathbf{r}}$ the lateral coordinates in the object plane, see Fig. 1), forms a random pattern in a remote image plane when a scattering medium is placed somewhere between these planes.

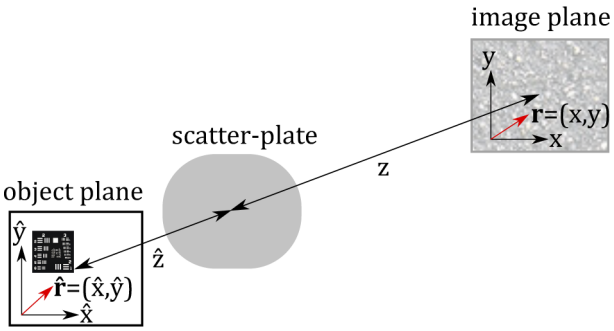

Fig. 1. Principle of SPM. A visually opaque scatter-plate is positioned between the object and the image plane. An image is retrieved from the recorded pattern via cross-correlation with the previously recorded PSF.

If the size of the object is restricted to the so-called memory effect area (within this area the memory effect holds true) the formation of the intensity pattern I_{ob} can be expressed by convolution, as it is the case for conventional imaging systems (e.g. lenses). For spatially incoherent sample illumination the pattern formation can be expressed by a convolution of intensities

$$I_{ob}(\mathbf{r}, z, \hat{z}) = \iint |S(\mathbf{r} - \hat{\mathbf{r}}, z, \hat{z})|^2 \, |O(\hat{\mathbf{r}}, \hat{z})|^2 \, \mathrm{d}\hat{\mathbf{r}} = |S(\mathbf{r}, z, \hat{z})|^2 * |O(\mathbf{r}, \hat{z})|^2 \ , \tag{1}$$

for spatially coherent illumination the pattern formation is determined by the convolution of the amplitudes

$$I_{ob}(\mathbf{r}, z, \hat{z}) = \left| \iint S(\mathbf{r} - \hat{\mathbf{r}}, z, \hat{z}) O(\hat{\mathbf{r}}, \hat{z}) \mathrm{d}\hat{\mathbf{r}} \right|^2 = |S(\mathbf{r}, z, \hat{z}) * O(\mathbf{r}, \hat{z})|^2 \ . \tag{2}$$

$S(\mathbf{r}, z, \hat{z})$ is the amplitude distribution in the image plane generated by a point source positioned in the origin of the object plane. We call the term $|S(\mathbf{r}, z, \hat{z})|^2$ the PSF of the scattering medium. z is the distance between the recording sensor and the scattering medium and $\mathbf{r}$ are the coordinates in the image plane (see Fig. 1). We consider z and $\hat{z}$ to be fixed.

In scatter-plate microscopy an image is retrieved by cross-correlating ($\star$) the recorded pattern with the previously recorded PSF. Since the PSF of a scattering medium is a speckle pattern, its auto-correlation $|S(\mathbf{r})|^2 \star |S(\mathbf{r})|^2$ is a sharply peaked function with a constant background of half

Optics EXPRESS

the peak's maximum value ($b = h$ in Fig. 2(a)). Because of the similarity to an Airy disc, the imaging capabilities of this approach is obvious in the case of spatially incoherent illumination:

$$I_{incoh}(\mathbf{r}) = \left[|O(\mathbf{r})|^2 * |S(\mathbf{r})|^2\right] \star |S(\mathbf{r})|^2 = |O(\mathbf{r})|^2 * \left[|S(\mathbf{r})|^2 \star |S(\mathbf{r})|^2\right] . \tag{3}$$

However, Freund could show that also for spatially coherent sample illumination this approach leads to an image. The auto-correlation of the fields $S(\mathbf{r}) \star S(\mathbf{r})$ is a sharply peaked function but now the constant background term is zero ($b = 0$ in Fig. 2(a)). Therefore, we can use the approximation $\int S(\mathbf{r}-\mathbf{r}')S(\mathbf{r})\mathrm{d}\mathbf{r}\mathrm{d}\mathbf{r}' \approx \delta(\mathbf{r}-\mathbf{r}')\int S(\mathbf{r})\mathrm{d}\mathbf{r}$ and demonstrate the equivalency between the coherent and the spatially incoherent illumination case:

$$\begin{aligned} I_{coh}(\mathbf{r}) &= |O(\mathbf{r}) * S(\mathbf{r})|^2 \star |S(\mathbf{r})|^2 = \left[\iint O(\mathbf{r}')S(\mathbf{r}'-\mathbf{r})O(\mathbf{r}'')S(\mathbf{r}''-\mathbf{r})\mathrm{d}\mathbf{r}'\mathrm{d}\mathbf{r}''\right] \star |S(\mathbf{r})|^2 \\ &\approx \left[\iint O(\mathbf{r}')O(\mathbf{r}'')\,|S(\mathbf{r}'-\mathbf{r})|^2\,\delta(\mathbf{r}''-\mathbf{r}')\mathrm{d}\mathbf{r}'\mathrm{d}\mathbf{r}''\right] \star |S(\mathbf{r})|^2 \end{aligned} \tag{4}$$

$$= \left[\iint |O(\mathbf{r}')|^2\,|S(\mathbf{r}'-\mathbf{r})|^2\,\mathrm{d}\mathbf{r}'\right] \star |S(\mathbf{r})|^2 = \left[|O(\mathbf{r})|^2 * |S(\mathbf{r})|^2\right] \star |S(\mathbf{r})|^2 \tag{5}$$

Instead of cross-correlating the pattern recorded with the sample in the object plane with a previously recorded PSF it is also possible to record the sample pattern and the PSF at once (by positioning a point source and the object within the memory effect range) and auto-correlate the recorded pattern. In the case of incoherent illumination one retrieves

$$\begin{aligned} I(\mathbf{r}) &= \left[\left(|O(\mathbf{r})|^2 + \delta(\mathbf{r}-\mathbf{r_0})\right) * |S(\mathbf{r})|^2\right] \star \left[\left(|O(\mathbf{r})|^2 + \delta(\mathbf{r}-\mathbf{r_0})\right) * |S(\mathbf{r})|^2\right] \\ &= \left[|O(\mathbf{r}+\mathbf{r_0})|^2 + |O(-\mathbf{r}-\mathbf{r_0})|^2 + |O(\mathbf{r})|^2 \star |O(\mathbf{r})|^2 + \delta(\mathbf{r})\right] * \left[|S(\mathbf{r})|^2 \star |S(\mathbf{r})|^2\right] . \end{aligned} \tag{6}$$

In the case of coherent sample illumination we apply the same approximation as in Eq. (4) and also end up with Eq. (6).

As mentioned the auto-correlation of the PSF is a sharply peaked function. That is why we have two mirrored images separated from the centre of the frame, which is dominated by the auto-correlation terms of the object and the PSF.

2.1. SPM through changing scatter-plates

Recording the sample pattern and the PSF at once and retrieve the image from the auto-correlation according to Eq. (6) makes SPM a true single shot imaging technique and therewith it opens up the possibility to image through moving or changing scattering media. We concentrate the discussion on just one of the twin image terms of Eq. (6) ($(|O(\mathbf{r}+\mathbf{r_0})|^2 * \left[|S(\mathbf{r})|^2 \star |S(\mathbf{r})|^2\right]$,valid for both spatially coherent and incoherent sample illumination). For moving or changing scatter-plates, the PSF becomes time-dependent. Recording the pattern within the integration time t_{int} the imaging term becomes

$$\begin{aligned} &|O(\mathbf{r}+\mathbf{r_0})|^2 * \left[\int_0^{t_{int}} |S(\mathbf{r},t)|^2\,\mathrm{d}t \star \int_0^{t_{int}} |S(\mathbf{r},t')|^2\,\mathrm{d}t'\right] \\ &= |O(\mathbf{r}+\mathbf{r_0})|^2 * \int_0^{t_{int}}\int_0^{t_{int}} |S(\mathbf{r},t)|^2 \star |S(\mathbf{r},t')|^2\,\mathrm{d}t\mathrm{d}t' = |O(\mathbf{r}+\mathbf{r_0})|^2 * K\left(S(\mathbf{r},t), t_{int}\right) . \end{aligned} \tag{7}$$

The influence of the variation in the scattering behaviour is contained in the convolution kernel $K\left(S(\mathbf{r},t), t_{int}\right)$. The integrand in the kernel term is the correlation of two speckle patterns. For now we discuss the kernel shape resulting from correlations between patterns of infinite size. This condition ensures that the kernel term is a peaked function with a smooth noiseless background. The consequence of finite sensing areas will be discussed later.

Optics EXPRESS

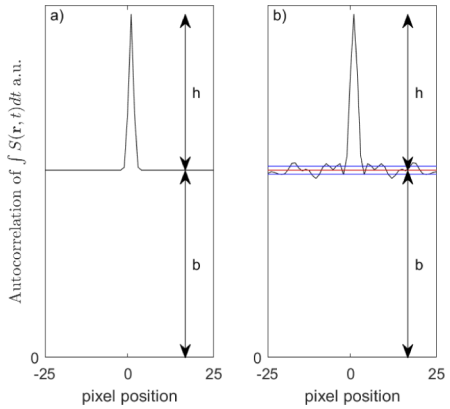

Fig. 2. Schematic illustration of the convolution kernel $K\left(S(\mathbf{r},t),t_{int}\right)$ (see Eq. (7), plotted along a line through the center of the pattern's auto-correlation. (a) With a theoretically infinite pattern area the background of the kernel is constant and no noise disturbs the image formation. (b) A finite sensor area results in a background noise. Data from simulation: sensor with 50×50 pixels and 5 µm pixel pitch, $\lambda = 532$ nm, $\hat{z} = z = 47$ mm, the temporal modulation was realized with 30 interpolation steps between two random phase arrays, see detailed description in section 3.1. b and the peak height h are now measured from the mean value of the background (red line). b is reduced significantly in the figure to reveal the structure of the convolution kernel (simulation result $\frac{h}{b} = 2 \cdot 10^{-3}$). σ_K is the standard deviation of the kernel's background noise. The blue lines indicate the values $b \pm 3\sigma_K$.

Further, we concentrate on the cases of separable time correlations. This is realized by phase-modulating scatter-plates (absorption coefficient $\sigma_a = 0$) when the phase changes at each position in the scatter-plate plane continuously in time, independently from spatially separated positions. Throughout the continuous phase change at each position, the statistic scattering behaviour shall not change (scattering coefficient σ_s remains unchanged). We call this a continuously and randomly changing scatter-plate. Experimentally such a scatter-plate is realized by a continuously rotating ground glass diffuser. We applied rotation velocities between $1\,^\circ\,\mathrm{s}^{-1}$ and $7\,^\circ\,\mathrm{s}^{-1}$ (see section 4.2). Fog or emulsions may also show a comparable scattering behaviour. However we have to mention that in such media inducing volume scattering rather than surface scattering (in the case of a ground glass diffuser, scattering is induced by a single rough surface), the range of the memory effect shrinks with the thickness of the scattering medium and in turn the imaging capabilities are limited.

The integrand of the kernel term in the case of infinite pattern sizes and separable time correlation becomes:

$$|S(\mathbf{r},t)|^2 \star |S(\mathbf{r},t')|^2 = \bar{I}\left(1 + |\mu(\mathbf{r},t)|^2\right) = \bar{I}\left(1 + |\mu(\mathbf{r})|^2\,\gamma(t-t')\right), \tag{8}$$

with $\bar{I}$ being the mean intensity of the patterns [15]. $\gamma(\tau)$ is a time correlation function with $\gamma(0) = 1$. For $|\tau| \to \infty$ γ tends towards zero. The correlation time Δt shall be the period in which the time correlation function falls below the value of $\frac{1}{e}$ (where e is Euler's number). $|\mu(\mathbf{r})|^2$ is the spatial correlation function, an Airy disc like function with $|\mu(0)|^2 = 1$ which goes for $|\mathbf{r}| \to \infty$ to zero. The width of its peak is determined by the numerical aperture of the setup. The kernel

Optics EXPRESS

can now be rewritten as:

$$\begin{aligned}\int_0^{t_{int}}\int_0^{t_{int}} |S(\mathbf{r},t)|^2 \star |S(\mathbf{r},t')|^2 \,\mathrm{d}t\mathrm{d}t' &= \bar{I}\left(t_{int}^2 + |\mu(\mathbf{r})|^2 \int_0^{t_{int}}\int_0^{t_{int}} \gamma(t-t')\mathrm{d}t\mathrm{d}t'\right) \\ &= \bar{I}\left(t_{int}^2 + 2\,|\mu(\mathbf{r})|^2 \int_0^{t_{int}}\int_0^{t'} \gamma(\tau)\mathrm{d}\tau\mathrm{d}t'\right).\end{aligned} \tag{9}$$

To obtain an insight into the dependence of the peak to background relation $\alpha = \frac{h+b}{b}$ (h peak height, b background value, see Fig. 2) on the integration time and the correlation time we simplify the problem and consider a time correlation function $\gamma(\tau)$ which shows perfect correlation for $|\tau|$ smaller than the correlation time Δt. For $|\tau| > \Delta t$ however the patterns shall be entirely decorrelated ($\gamma(\tau) = 1$ for $0 \le \tau \le \Delta t$, otherwise $\gamma(\tau) = 0$). For $\Delta t < t_{int}$ such a correlation function gives

$$\int_0^{t_{int}}\int_0^{t_{int}} |S(\mathbf{r},t)|^2 \star |S(\mathbf{r},t')|^2 \,\mathrm{d}t\mathrm{d}t' = \bar{I}\left(t_{int}^2 + |\mu(\mathbf{r})|^2\left(2t_{int}\Delta t - \Delta t^2\right)\right). \tag{10}$$

With $\max\left(|\mu(\mathbf{r})|^2\right) = 1$ we obtain the peak to background relation

$$\alpha = \frac{t_{int}^2 + 2t_{int}\Delta t - \Delta t^2}{t_{int}^2} = 1 + 2\frac{\Delta t}{t_{int}} - \frac{\Delta t^2}{t_{int}^2}. \tag{11}$$

In the case of a static (not changing) scatter-plate the correlation remains over the whole integration time ($\Delta t = t_{int}$) and the peak to background ratio is $\alpha = 2$. Nevertheless even for integration times much greater than the correlation time a peak to background ratio greater than one remains. Since a constant background in the convolution kernel does not disturb imaging (see Fig. 3), also in the case of changing scatter-plates SPM should be realizable.

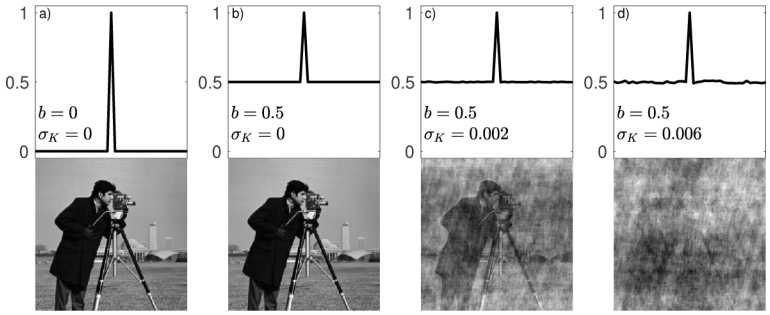

Fig. 3. Influence of the background value b and the kernel noise σ_K on the image quality. The cameraman image was convolved with the artificial kernels shown in the upper figures. (a) The convolution with an Airy disk like kernel has little effect on the image quality. (b) The constant background b in the kernel has no worsening effects. (c) and (d) We added white background noise to the kernel. The presence of a background noise disturbs the image considerably. In SPM the kernel involved in the image formation always carries noise. The relation $\frac{h}{\sigma_K}$ determines the image quality and depends on the number of recorded speckles and consequently on the size of the sensor area and on the speckle size.

Since the patterns used for image retrieval are recorded on a restricted sensor area, the background of the kernel is not constant but shows some noise (see Fig. 2). Therefore, the background value b is in the experimental realisation just the mean value of the kernel background. The background fluctuations reduce the image quality (see Fig. 3). However, we could demonstrate

Optics EXPRESS

via simulation that the relation of the peak height h and the standard deviation of the background noise σ_K depends on the size of the recorded pattern but not on the relation between integration time t_{int} and the correlation time Δt (see Fig. 11 in section 4.2). Consequently, the noise does disturb imaging in the case of a changing scatter-plate just as much as in the case of a static scatter-plate. What really restricts the capability of SPM to image through rotating diffusers is therefore just the specifications of the recording system. Especially the dynamic range and the bit depth of the camera limit the imaging through changing scatter plates. The influence of the finite pixel size is not taken into account in this publication. This is consistent as long as the average speckle size is much larger than the pixel size.

In SPM, the speckle size is in a wide range proportional to the wavelength and the magnification and decreases with increasing NA. By choosing suitable values for the distance between the object plane and the scattering medium and the distance between the scattering medium and the sensor or by limiting the illuminated scattering area with a diaphragm, an appropriate resolution of the speckle pattern can be ensured (see Supplement 1 for detailed information).

To obtain a peak structure in the kernel (Eq. (7)) the contrast of the pattern $\int_0^{t_{int}} S(\mathbf{r}, t)\mathrm{d}t$ must be detected. In the following, we estimate some restrictions on the relation between integration time and correlation time, which must be fulfilled to realize imaging through changing scatter-plates. We assume the contrast of the intensity pattern resolved, if its standard deviation and its mean intensity fulfil the relation

$$t_{int}(\sigma_I + \bar{I}) < E_{max}\,. \tag{12}$$

E_{max} is the maximum energy a pixel of the sensor can record without being saturated. This value is determined by the maximum dynamic range the sensor can cover. For a given mean intensity $\bar{I}$ we define the maximum integration time by $t_{maxint} = \frac{E_{max}}{\bar{I}}$. With the definition of the speckle contrast $C = \frac{\sigma_I}{\bar{I}}$ [15], Eq. (12) becomes

$$C + 1 < \frac{t_{maxint}}{t_{int}}\,. \tag{13}$$

Due to the finite bit depth of the sensor, the recorded patterns have discrete values. Considering the bit depth N, the contrast is detectable, if the system fulfils the condition:

$$t_{int}\sigma_i > \frac{E_{max}}{2^N - 1}\,. \tag{14}$$

For a given mean intensity, the contrast must satisfy

$$C > \frac{t_{maxint}}{t_{int}(2^N - 1)} \tag{15}$$

and we obtain the imaging condition

$$\frac{t_{maxint}}{t_{int}(2^N - 1)} < C < \frac{t_{maxint}}{t_{int}} - 1\,. \tag{16}$$

For a uniform time integration the contrast can be expressed as

$$C = \left[\frac{2}{t_{int}}\int_0^{t_{int}} \left(1 - \frac{\tau}{t_{int}}\right)\gamma(\tau)d\tau\right]^{\frac{1}{2}}\ [15]\ . \tag{17}$$

If we choose again the correlation function $\gamma(\tau) = 1$ for $0 \le \tau \le \Delta t$ (otherwise $\gamma(\tau) = 0$) and $\Delta t < t_{int}$ we end up with

$$\frac{t_{maxint}}{2^N - 1} < \left[2t_{int}\Delta t - \Delta t^2\right]^{\frac{1}{2}} < t_{maxint} - t_{int}\,. \tag{18}$$

The argument of the square root $2t_{int}\Delta t - \Delta t^2$ represents the peak height in Eq. (11). The result in Eq. (18) gives a minimal condition, which must be fulfilled to apply SPM in the configuration

Optics EXPRESS

described by Eq. (6) (sample pattern and PSF recorded at once). However, we want to emphasize that in our consideration just the contrast of the kernel was taken into account. Depending on the sample and whether its illumination is spatially coherent or incoherent, the contrast of the recorded pattern might be reduced drastically compared to the contrast assumed by Eq. (17). Higher pattern contrast and therefore the better imaging conditions for SPM is expected for rather sparse samples [8].

3. Simulation and experimental setup

3.1. Simulation of Scatter-Plate Microscopy

We simulated SPM to investigate its imaging capabilities for coherent and spatially incoherent sample illumination. To simulate scattering media we created square random phase arrays M from a uniform distribution:

$$M = \exp\left(2\pi i \cdot X_{[0,1]}\right) \tag{19}$$

with $X_{[0,1]}$ being an array of uniformly distributed random numbers between zero and one. In the case of SPM with coherent sample illumination, we applied Fresnel approximation to propagate the field from the object plane to the scatter-plate plane:

$$E_{out}(x,y,z) = \frac{\exp\left[ik\left(z-z'\right)\right]}{i\lambda\left(z-z'\right)} \int\int_{-\infty}^{\infty} E_{in}\left(x',y',z'\right) e^{\frac{ik}{2z}\left[(x-x')^2+(y-y')^2\right]} \mathrm{d}x'\mathrm{d}y', \tag{20}$$

with (x', y', z') the coordinates in the object plane and (x, y, z) the coordinates in the scatter-plate plane. Since we simulate on discrete meshes we applied the Fast Fourier Transformation (FFT) on both the distribution $E_{in}(x'_{ij}, y'_{ij}, z'_{ij})$ and on the convolution kernel $\exp\left[\frac{ik}{2z}\left(x_{ij}^2 + y_{ij}^2\right)\right]$ to subsequently calculate this convolution in Fourier space (in Fourier space a convolution becomes a multiplication). The resulting field distribution in the scatter-plate plane is multiplied with the random phase array M and afterwards another Fresnel propagation is applied to obtain the resulting scattered field and subsequently the intensity distribution in the image plane.

To simulate the point source illumination we used a spherical wavefront

$$E_{out}(x,y,z) = \frac{E_0}{r}\exp\left(ikr\right) \tag{21}$$

with $r = \left[(x-x')^2 + (y-y')^2 + (z-z')^2\right]^{1/2}$ to calculate the field distribution in the scatter-plate plane. (x', y', z') marks in this context the point source position.

Spatially incoherent illumination was simulated by adding the speckle fields generated by each nonzero point in the object plane. Since in the case of incoherent sample illumination the object is approximated as a cluster of point sources we perform in our simulations SPM with magnification $M = 1$ to prevent the image points driving apart. To avoid any spurious effects from the FFT the object was padded with zeros and the scattering area of the random phase array was reduced with a circular aperture. Furthermore to obtain a realistic intensity distribution in the image plane we ensured critical sampling for the Fresnel-propagation meaning $\Delta x = \frac{\lambda z}{L}$, with Δx the sample interval (pixel pitch) and L the side length in the spatial domain (sensor size), z the propagation distance and λ the wavelength [16].

As mentioned in our understanding a continuously but randomly changing scatter-plate changes its scattering behaviour at each position continuously but independent from the changing behaviour at all other positions. To simulate such a change in the random phase we created two arrays of random numbers $X^{(1)}_{[0,1]}$ and $X'_{[0,1]}$ and calculated their sum:

$$X^{(2)} = X^{(1)}_{[0,1]} + X'_{[0,1]} \tag{22}$$

Now we further interpolate linearly and pixelwise between the arrays $X^{(1)}_{[0,1]}$ and $X^{(2)}$. For all pixels we choose the same number of interpolation steps n_{int}. By this we obtain a set of

Optics EXPRESS

random number arrays simulating a continuous transition from $X^{(1)}_{[0,1]}$ to $X^{(2)}$. The procedure can be continued by creating a further random number array $X''_{[0,1]}$, calculating its sum with $X^{(2)}$, interpolating between the result and $X^{(2)}$ and so on. With Eq. (19), all arrays of the set result in a uniform phase distribution.

To simulate intensity patterns generated with randomly but continuously changing scatter-plates we have to calculate the intensity patterns for each random number array of the set separately and finally building the sum of these patterns pixelwise. If we have N patterns for this sum then the relation $\frac{n_{int}}{N}$ gives the relation between the correlation time and the integration time $\frac{t_{coh}}{t_{int}}$.

3.2. Experimental setup and image acquisition

Figure 4 shows the experimental setup for SPM with coherent (a) and incoherent (b) sample illumination. We choose a setup, which enables to record the sample pattern and the PSF at once in a single shot approach. Images were therefore retrieved via auto-correlation. We used a frequency-doubled Nd:YAG-laser with a wavelength of 532 nm as light source. To approximate a point source, we used an SM-fibre with NA=0.15 and positioned the fibre tip close to the sample in the object plane (within the memory effect range of the sample region). An alternative realization of a point source-like light-source would be a laser beam focused into the objet plane [14]. A single nanoparticle in the object plane illuminated to irradiate spherically with the desired wavelength could make the method even more suitable for practical applications.

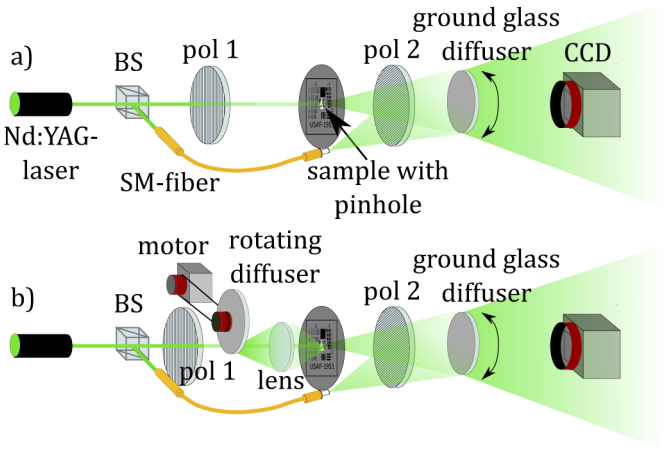

Fig. 4. Experimental setup for SPM. PSF and sample pattern are recorded at once and the image is retrieved by auto-correlating the recorded pattern. A single mode fibre serves as a point source-like light source. The field of view is restricted by a pinhole. (a) SPM with coherent sample illumination: the intensity of the laser beam is adjusted by two polarizers to fit the intensity of the sample illumination to the intensity emitted by the SM-fibre. (b) SPM with spatially incoherent illumination: the laser beam is lead through a rotating ground glass diffuser to destroy spatial coherence. A lens images the spot on the rotating diffuser onto the region of interest. In the case of spatially incoherent sample illumination the intensity of the SM-fibre is fit to the sample illumination by adjusting the fibre coupling.

The patterns were recorded with a CCD-Camera from VISTEK-GMBH with 4384×6576 pixels and a pixel size of 5.5 µm×5.5 µm. A diaphragm between the scatter-plate and the object determined the NA (not in Fig. 4). Two polarizers are used to adjust the intensity of the sample illumination. To realize spatially incoherent sample illumination, the laser beam was let through a rotating ground glass diffuser and a lens (f = 70 mm, diameter D = 40 mm). For spatially

Optics EXPRESS

coherent sample illumination the rotating ground glass diffuser and the collimating lens were removed from the beam path and the laser beam illuminated directly the sample.

Our scatter-plate was a THORLABS DG-600 ground glass diffuser. In order to realize imaging with different diffuser orientations and with a continuously changing scattering media the diffuser was mounted on a rotation stage.

The recorded patterns carry a so-called scattered light envelope [17]. This low frequency intensity variation affects the calculated auto-correlations and disturb the imaging. To reduce the effect of the envelope we performed a shading correction by subtracting from the recorded patterns low-pass filtered versions of themselves. For coherent illumination, depending on the illumination strength and the sparsity of the sample it may also become necessary to remove a bright spot in the pattern caused by the ballistic unscattered photons.

We imaged the central part of the 1951 USAF resolution test chart and onion cells. The FOV was restricted by a 800 µm pinhole in the case of the USAF chart and a 400 µm pinhole in the case of the onion cells.

4. Results

4.1. SPM with Spatially Coherent and Incoherent Sample Illumination

The results of SPM-simulations are shown in Fig. 5. We applied the same sampling interval $\Delta x = 5$ mm in the object plane, in the scatter plane and in the image plane. The three planes were simulated with 5000×5000 pixels leading to a side length $L = 25$ mm. Simulating with a wavelength of $\lambda = 532$ nm and applying critical sampling the distance between the object plane and the scatter plane as well as the distance between the scatter plane and the image plane became $z = 235$ mm (magnification $M = 1$). In the scatter plane a circular aperture was applied (diameter $d = 10$ mm, $NA = 0.021$). (b-c) and (e-f) were retrieved with a single diffuser, for (d) and (g) 100 images retrieved with different diffusers were averaged. For the images (b), (d), (e) and (g) just the central region of the patterns (500×500 pixels) were taken into account for cross-correlation. The images (c) and (f) were retrieved with 5000×5000 pixels.

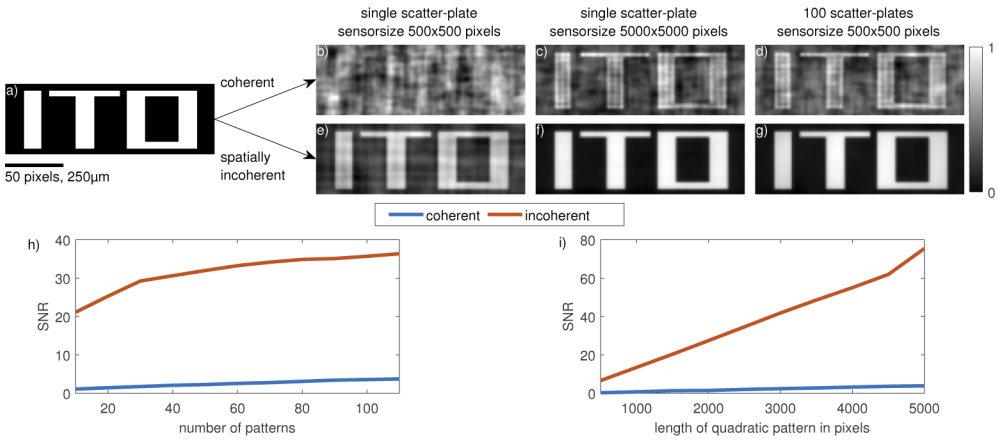

Fig. 5. Simulation of scatter-plate microscopy with (b-d) coherent and with (e-g) spatially incoherent sample illumination (detail views). (a) binary ITO-lettering used as sample. (h) Dependence of the SNR on the number of patterns used for image retrieval (pattern size 500×500 pixel). (i) Dependence of the SNR on the pattern size (image retrieved from a single pattern).

The simulation result shown in Fig. 5(b) reveals one of the reasons why SPM with coherent illumination was so far not realized: To obtain an adequate signal-to-noise ratio with coherent

Optics EXPRESS

sample illumination and a single scatter-plate, comparatively large parts of the generated patterns have to be recorded. For spatially incoherent illumination, on the other hand a much smaller sensor size is appropriate for imaging with a single scatter-plate. However, Fig. 5(d) shows that due to the ergodicity between the spatial cross-correlation and the ensemble average the necessity of very large sensors can be overcome by averaging over the results obtained with many different scatter-plates.

To show how the image quality depends on the number of patterns and the pattern-size we calculated the signal-to-noise ratio $SNR = (S1 - S2)/\sigma_b$ (Fig. 5(h-i)), with S_1 the average image value of the ITO-letter-area, S_2 the average of the image background and σ_b the standard deviation of the image background.

In the experimental realization, we implemented the averaging over different scatter-plates by step-rotating a ground glass diffuser and by this we recorded patterns with many different diffuser orientations. Better results are expected when at first the sample patterns are recorded for the different diffuser orientation and then afterwards the PSF are recorded for exactly the same diffuser orientations with now the point source in the former position of the sample. With this approach the image is retrieved by cross-correlating the corresponding recordings followed by the averaging of these correlations. However, such an approach needs a strong stability of the setup. Especially the diffuser orientations needed to be reproducible with high accuracy. Therefore, we preferred to apply the approach described by Eq. (6) in which the PSF and the sample pattern are recorded at once. A drawback of this approach is that a lateral distance between the sample position and the point source position becomes unavoidable (in the image the region around the point source position is dominated by the object's auto-correlation) leading to a loss of image quality due to a reduced memory effect.

When PSF and sample pattern are recorded at once it is essential that the intensity irradiated by the objects fits well to the intensity of the point source. Otherwise, the image is not or at least not well retrieved in the auto-correlation of the pattern. Figure 6 demonstrates how the relation between these intensities affects the image quality. In the simulation, the lateral distance between point source and sample was set to 5 mm. The results were obtained by averaging over 100 images acquired with different random diffusers. Other simulation parameters are chosen as in Fig. 5. The best result (c) is achieved with a point source amplitude E_{opt} that makes the point source's energy flux through the aperture equal to the energy flux of the sample. Higher or lower values of E_0 reduce the signal-to-noise ratio (Fig. 6(b) and (d)).

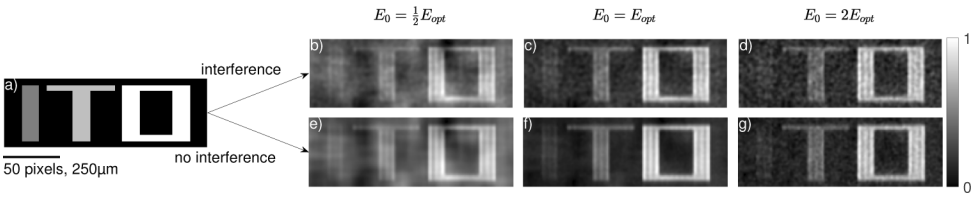

Fig. 6. Simulation of scatter-plate microscopy with coherent sample illumination. The point source and the sample illuminate the scatter-plate simultaneously. Images were retrieved via auto-correlation. (b-d) the field generated by the point source and the field generated by the sample interfered in the image plane. (e-g) the fields did not interfere. Detail views of results obtained with different point sources amplitudes E_0 are shown. For both interfering and not interfering fields, best results (c) are achieved with a point source amplitude E_{opt} that makes the point source's energy flux through the aperture equal to the energy flux of the sample. The field distribution in the object plane (a) is real, but not binary.

If the PSF and the sample pattern are recorded at once and the sample is illuminated coherently, interference effects between the two fields in the sensor plane may affect the image quality. In Fig. 6(e-g), we artificially suppressed the interference effects and just added the intensity

Optics EXPRESS

distributions generated by the two fields separately. The image quality is slightly better, but the necessity to adjust the point source amplitude to the energy flux of the sample remains crucial.

4.1.1. Experimental results

Figure 7 shows images of the USAF-target and of a piece of onion-cells we retrieved with SPM and static diffusers. To be able to average over results obtained with different scatter-plates the diffuser was rotated between two pattern recordings (but not during a recording). We recorded the PSF and the sample at once. The distance between the diffuser and the object was 104 mm, the distance between the diffuser and the CCD was 210 mm (onion cells) respectively 310 mm (USAF-target) resulting in a magnification of $M = 2.02$ respectively $M = 3.07$. The distance between the tip of the fibre and the center of the object was 4.4 mm in the case of the USAF-target and 8.7 mm in the case of the onion cells. Figure 7(e), (i), (n) and (r) show images recorded with a single lens (focal length $f = 80$ mm, diameter $D = 40$ mm) and the same magnification. For both imaging with the SPM and imaging with the lens the NA was restricted by a diaphragm to 0.1.

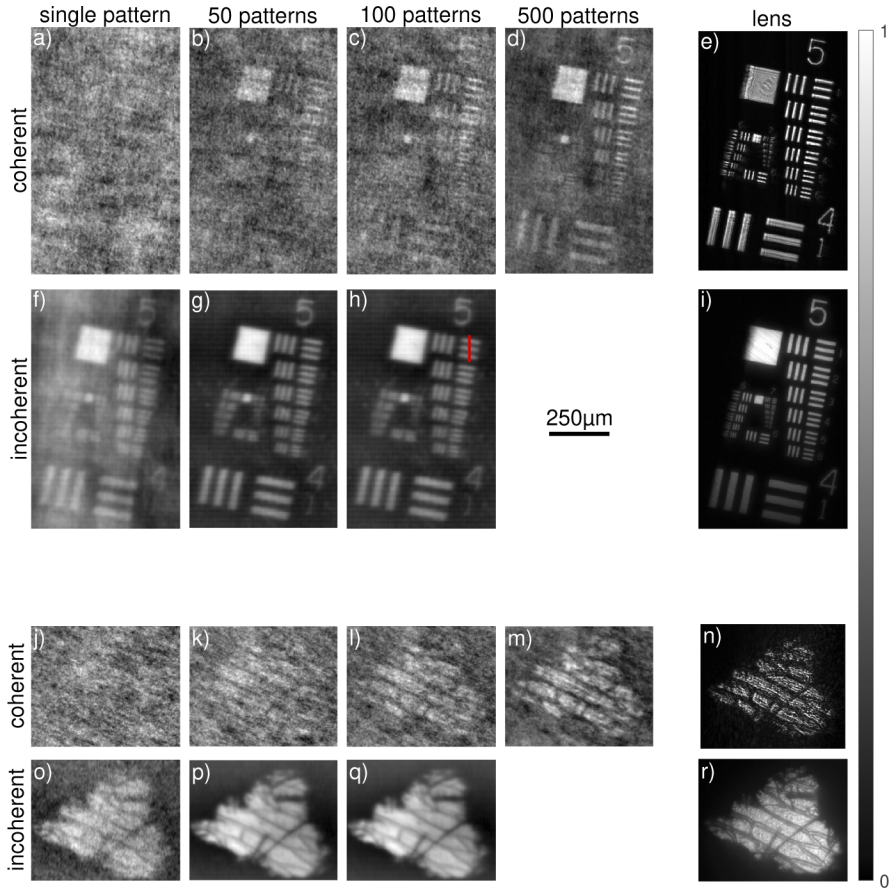

Fig. 7. Scatter-plate imaging results with static ground-glass diffusers. Detail views of images of the (a-i) USAF-target and of (j-r) onion cells retrieved by averaging over(a,f,j,o) single (b,g,k,p) 50, (c,h,i,q) 100 patterns and in the case of coherent sample illumination also over (d,m) 500 images. (e), (i), (n) and (r) show images recorded with a single lens and the same magnification and NA. The red line in h) refers to the cross line profiles in Fig. 9

Optics EXPRESS

While for incoherent sample illumination a single pattern is enough to reveal object details in the reconstruction and an average over more than 50 images does not lead to further improvement, for coherent sample illumination an averaging over far more than 100 results is necessary to retrieve an acceptable result. However, with incoherent sample illumination the retrieved images show a much better signal-to noise-ratio, a better resolution and a better contrast. Figure 8 shows how the SNR of the USAF-target images depend on the number of patterns used for image retrieval for both spatially coherent and spatially incoherent sample illumination. Cross line profiles through USAF-target element 1 in group 5 are shown in Fig. 9(a-b) comparing the image resolution.

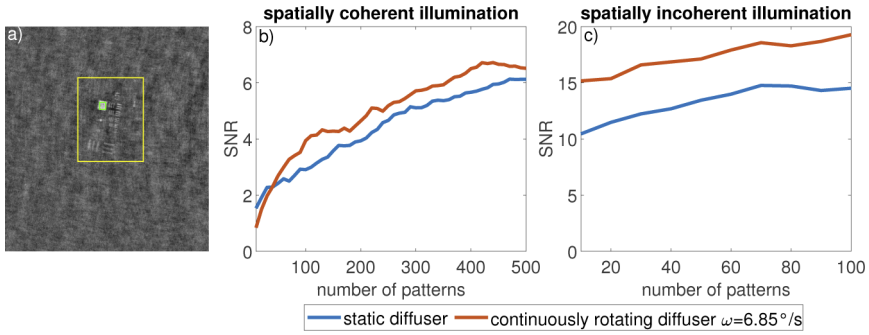

Fig. 8. Signal-to-noise ratio $SNR = (S1 - S2)/\sigma_b$ in dependence on the number of patterns. (a) Detail view of the image retrieved with coherent illumination, 500 patterns and static diffuser (see Fig. 7(d)). The image shows how we determined $S1$, $S2$ and σ_b: $S1$ is the average image value within the green rectangle, $S2$ the average value outside the yellow rectangle and σ_b the standard deviation outside the yellow rectangle. (b) for spatially coherent sample illumination and (c) for spatially incoherent sample illumination. The SNR is plotted for USAF-target images retrieved with static respectively with continuously rotating ground glass diffuser.

4.2. *Changing scatter-plates*

To realize a continuously but randomly changing scatter-plate experimentally we let a ground glass diffuser rotate during the recording of the patterns. In Fig. 10 we compare the decorrelation of the PSF's speckle pattern recorded with a rotating diffuser (b) with the decorrelation of a simulated PSF-pattern of a random phase mask which changes its phase at each pixel position randomly but continuously (a). For the simulation we computed the pattern generated by a random phase mask with just a point source in the object plane ($NA = 0.02$, distance scatter-plate to object respectively to image plane 47 mm, pixel pitch 5 µm, 300×300 pixels) . Then we simulated patterns generated by phase masks, which result from the original mask by a random and continuous change (see section 3.1). Between two uncorrelated random masks, we interpolated 50 steps. For each pattern, we determined the peak value of the cross-correlation with the starting pattern. Finally, the cross-correlations were normalized to the auto-correlation peak value of the starting pattern.

The experimentally determined decorrelation was obtained by recording patterns generated by a ground glass diffuser. An SM-fibre served as a point source. The diffuser was rotated step-wise and the peak value of the cross-correlation with the starting pattern was determined. The cross-correlations were normalized to the auto-correlation peak value of the starting pattern. The decorrelation of the patterns generated with rotating diffuser (b) show a continuous decline from one to zero, just as the decorrelation in the simulation (a). The similarity between the correlations justify our assumption that a rotating diffuser is an adequate approximation of a continuously and randomly changing scatter-plate.

Optics EXPRESS

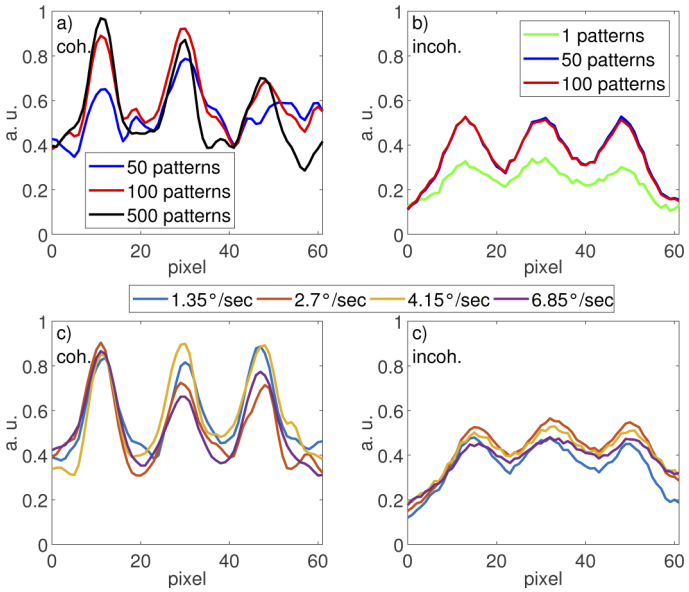

Fig. 9. Cross line profiles through USAF-target element 1 in group 5 along the red line in Fig. 7 (h). Imaging with static ground glass diffuser and (a) coherent illumination, respectively (b) incoherent illumination. Profiles are shown in dependence of the number of patterns used for image retrieval. (c-d) Imaging with continuously rotating ground glass diffuser. Profiles were retrieved with (c) 500 patterns with coherent illumination and (d) 100 patterns with incoherent illumination.

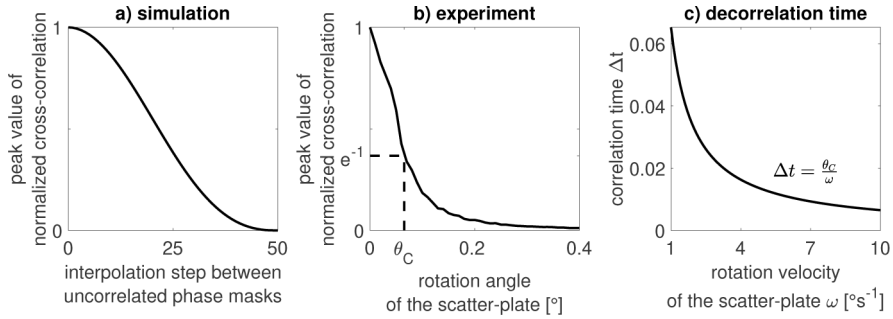

Fig. 10. Decorrelation of the PSF. (a) Decorrelation simulated with randomly but continuously changing phase masks, (b) decorrelation of the PSF of a rotating ground glass diffuser, c) dependence of the correlation time on the rotation velocity, with θ_C the correlation angle derived from the plot in (b).

In Fig. 11, we analyse the relation between the height of the PSF's auto-correlation peak and the standard deviation of its background for a rotating ground glass diffuser and simulated randomly changing scatter-plates. (a-c) show the relation between the peak height of the autocorrelation and the standard deviation of its background noise: we simulated PSFs generated with randomly but continuously changing phase masks (see Eq. (19) and 20, $NA = 0.02$, distance scatter-plate to object respectively to image plane 47 mm, pixel pitch 5 µm, 1000×1000 pixels). Between two random masks, we interpolated with 30 masks. To simulate a recording while the change of the scatter-plate we summed over the generated patterns. Different numbers of batched intensity patterns were summed up to simulate different integration times. Without any pixel saturation or

Optics EXPRESS

binarization in the simulation, the relation between the auto-correlation's peak height and the standard deviation of its background proves to be independent from integration time (a). In 10(b), we introduced a saturation intensity and a binarization of 256 intensity levels in the simulation. For small integration times the ratio drops rapidly. For higher integration times the saturation leads to a decrease of the ratio. In between the ratio remains constant enabling imaging with SPM. Figure 10(c) show the $\frac{h}{\sigma_K}$-ratio of the autocorrelation of the PSF generated by rotating ground glass diffusers. The curve shows a trend similar to the one in Fig. 10(b). Before the saturation becomes dominant, there is a range in which the ratio and therefore the imaging quality of SLM is more or less independent from the integration time. Figure 10(d-h) finally show the PSF's auto-correlation peak for different integration times. The peak height and the background level increase with the integration time but nevertheless there are distinct peak structures and the background fluctuation are not more pronounced.

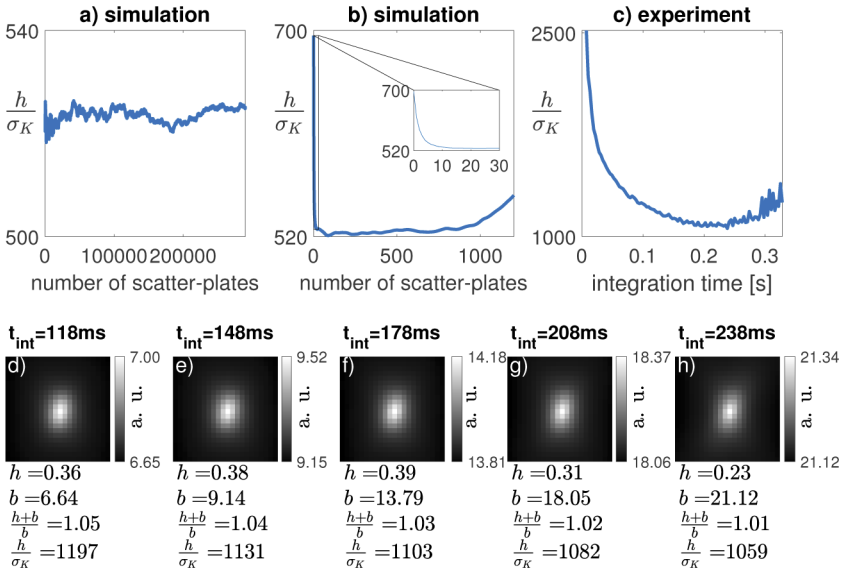

Fig. 11. Relation between peak height and standard deviation of the background fluctuations in the auto-correlation of the PSF. (a) We simulated speckle patterns of a point source generated with randomly but continuously changing phase masks (see Eq. (19) and 20). To simulate a recording while the change of the scatter-plate we summed over the generated patterns. Different numbers of batched intensity patterns were summed up to simulate different integration times. (b) We integrated a saturation intensity and a binarization of 256 intensity levels. (c) $\frac{h}{\sigma_K}$-ratio of the PSF's auto-correlation generated by rotating ground glass diffusers. (d-h) PSF's auto-correlation peak for different integration times. The peak height and the background level increase with the integration time but nevertheless there are distinct peak structures and the background fluctuation are not more pronounced.

Consequently, both the simulation and the experiment proof that the relation between the peak height and the standard deviation of the background noise does not depend on the integration time as long as the bin depth and the maximum dynamic range of the camera enables well resolved recording of the intensity pattern. If the integration time is neither too short (intensity range is not resolved due to the binarization of the signal) nor too long (saturation of the pixels) the rotation respectively the change of the scatter-plate should therefore have no negative influence on the imaging capabilities of the SPM when object pattern and PSF are recorded at once. The actual appropriate range of integration time depends on the intensity irradiated by the object and the point source.

Optics EXPRESS

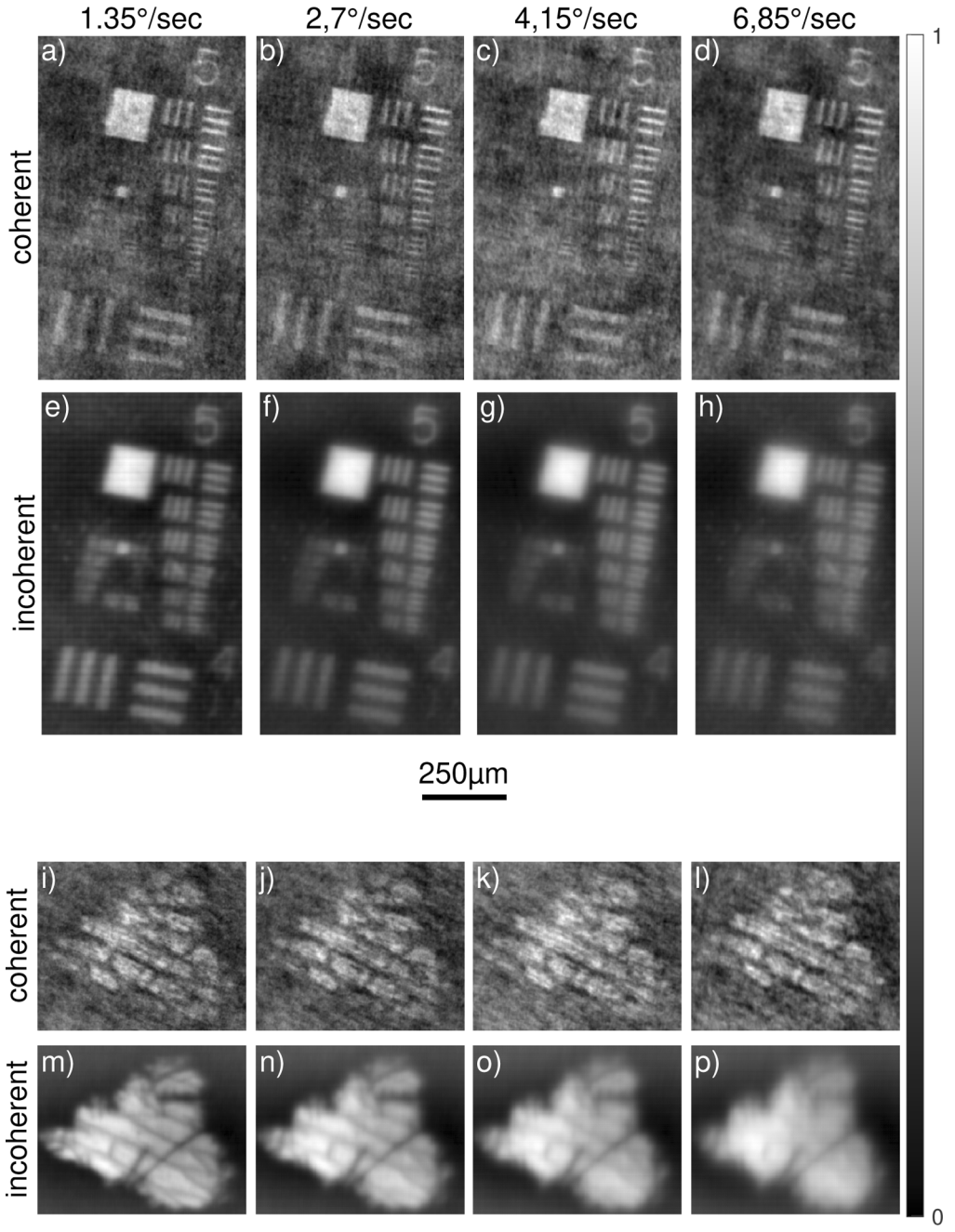

Fig. 12. Scatter-plate imaging with continuously rotating ground-glass diffusers. Detail views of images of the (a-h) USAF-target and of (i-p) onion cells retrieved by averaging over (a-d, i-l) 500, respectively (e-h, m-p) 100 patterns.

Optics EXPRESS

Figure 12 shows the images of the USAF-target and of the onion cells retrieved with ground-glass diffusers rotating during the recording of the patterns. Instead of different integration times, we applied different rotation velocities to investigate the imaging capabilities. The integration times were set to 8 ms (a-d and i-l), 600 ms (e-h) and respectively 120 ms (m-p) to avoid any saturation of the pixels. The NA, the distances between the diffuser and the object plane, respectively the distance between the diffuser and the CCD and the distances between the tip of the SM-fibre and the centre of the objects were set as in Fig. 7 for both the onion cell imaging and the USAF-target imaging.

Figure 8 shows how the SNR of the USAF-target images depend on the number of patterns used for image retrieval for both spatially coherent and spatially incoherent sample illumination. Especially in the case of coherent sample illumination, the rotation of the diffuser prove to have little influence on the image quality. This verifies that in the auto-correlation of the PSF the ratio between the peak height and the standard deviation of the background fluctuations does not depend on whether the scatter-plate is changing or not.

In the case of spatially incoherent sample illumination, Fig. 8(b) shows an even higher SNR for recordings with a continuously rotating diffuser. This is because the image region we used to calculate the SNR (see Fig. 8(a)) appears very bright in the images obtained with continuously rotating diffusers and spatially incoherent sample illumination. However, in the case of incoherent sample illumination both the USAF-target images (Fig. 12(h), but especially the images of the onion cells (Fig. 12(p)) show a lower resolution for high rotation speeds. The onion cells are far less sparse than the USAF-target leading to a reduced contrast in the recorded patterns especially in the case of short correlation times. According to our considerations in section 2.1, this leads to reduced performance of the SPM.

Figure 9(c-d) show cross line profiles through USAF-target element 1 in group 5, comparing the resolution of images acquired with rotating diffusers with both spatially coherent and spatially incoherent illumination.

5. Conclusion

We realized SPM as true single-shot imaging technique and avoided the separate recording of the scatter-plate's PSF. With this approach we could demonstrate that SPM is not only applicable with incoherent but also with coherent sample illumination. However, to achieve a comparable image quality with coherent illumination either one has to record a large area of the pattern or one has to average over images acquired with hundreds of scatter-plate realizations. Additionally, we could demonstrate that it is crucial to adjust the relation between the intensity irradiated by the sample and the intensity of the point source.

Our single-shot technique makes SPM further applicable for continuously and randomly changing scatter-plates. We demonstrated that a rotating ground glass diffuser could be regarded as an experimental realization of such a scatter-plate and demonstrated the performance of SPM with the rotating diffuser. Since also smog, emulsions or organic tissues could prove to be realizations of our concept of a randomly and continuously changing scattering medium, our approach can set up new applications to scatter-plate microscopy.

Funding. Chinesisch-Deutsche Zentrum für Wissenschaftsförderung (GZ 1391); Deutsche Forschungsgemeinschaft (Os 111/49-1).

Disclosures. The authors declare no conflicts of interest.

See Supplement 1 for supporting content.

References

1. J. Fade, S. Panigrahi, A. Carré, L. Frein, C. Hamel, F. Bretenaker, H. Ramachandran, and M. Alouini, "Long-range polarimetric imaging through fog," Appl. Opt. **53**(18), 3854–3865 (2014).
2. S. Sudarsanam, J. Mathew, S. Panigrahi, J. Fade, M. Alouini, and H. Ramachandran, "Real-time imaging through strongly scattering media: seeing through turbid media, instantly," Sci. Rep. **6**(1), 25033 (2016).

Optics EXPRESS

3. I. M. Vellekoop and A. P. Mosk, "Focusing coherent light through opaque strongly scattering media," Opt. Lett. **32**(16), 2309–2311 (2007).
4. J. M. Dela Cruz, I. Pastirk, M. Comstock, V. V. Lozovoy, and M. Dantus, "Use of coherent control methods through scattering biological tissue to achieve functional imaging," Proc. Natl. Acad. Sci. U. S. A. **101**(49), 16996–17001 (2004).
5. I. Freund, "Looking through walls and around corners," Phys. A **168**(1), 49–65 (1990).
6. I. Freund, M. Rosenbluh, and S. Feng, "Memory effects in propagation of optical waves through disordered media," Phys. Rev. Lett. **61**(20), 2328–2331 (1988).
7. J. R. Fienup, "Phase retrieval algorithms: a comparison," Appl. Opt. **21**(15), 2758–2769 (1982).
8. O. Katz, P. Heidmann, M. Fink, and S. Gigan, "Non-invasive single-shot imaging through scattering layers and around corners via speckle correlations," Nat. Photonics **8**(10), 784–790 (2014).
9. J. Bertolotti, E. G. van Putten, C. Blum, A. Lagendijk, W. L. Vos, and A. P. Mosk, "Non-invasive imaging through opaque scattering layers," Nature **491**(7423), 232–234 (2012).
10. I. M. Vellekoop and C. M. Aegerter, "Scattered light fluorescence microscopy: imaging through turbid layers," Opt. Lett. **35**(8), 1245–1247 (2010).
11. X. Xu, X. Xie, H. He, H. Zhuang, J. Zhou, A. Thendiyammal, and A. P. Mosk, "Imaging objects through scattering layers and around corners by retrieval of the scattered point spread function," Opt. Express **25**(26), 32829–32840 (2017).
12. A. K. Singh, D. N. Naik, G. Pedrini, M. Takeda, and W. Osten, "Exploiting scattering media for exploring 3d objects," Light: Sci. Appl. **6**(2), e16219 (2017).
13. A. K. Singh, G. Pedrini, M. Takeda, and W. Osten, "Scatter-plate microscope for lensless microscopy with diffraction limited resolution," Sci. Rep. **7**(1), 10687 (2017).
14. S. L. Ludwig, B. Le Teurnier, G. Pedrini, X. Peng, and W. Osten, "Image reconstruction and enhancement by deconvolution in scatter-plate microscopy," Opt. Express **27**(16), 23049–23058 (2019).
15. J. W. V. Goodman, ed., *Speckle phenomena in optics: theory and applications* (Roberts, Englewood, Colo, 2007).
16. D. V. Voelz, ed., *Computational Fourier optics: a MATLAB tutorial*, Tutorial texts in optical engineering ; 89 (SPIE Press, Bellingham, Wash, 2011).
17. M. Liao, D. Lu, W. He, G. Pedrini, W. Osten, and X. Peng, "Improving reconstruction of speckle correlation imaging by using a modified phase retrieval algorithm with the number of nonzero-pixels constraint," Appl. Opt. **58**(2), 473–478 (2019).